Statistical scaling of geometric characteristics in stochastically generated pore microstructures

Jeffrey D. Hyman[1] · Alberto Guadagnini[2,3] · C. Larrabee Winter[4]

Received: 23 October 2014 / Accepted: 23 April 2015 / Published online: 21 May 2015

1 Introduction

Computational simulations of flow through explicit porous microstructures allow for the detailed investigation of the way variations in pore wall geometry and pore network topology influence flow and transport at both microscopic and macroscopic scales. These numerical simulations can complement laboratory experiments to provide additional insights into how the rich pore-scale physics influence continuum-scale behaviors observed in both natural and industrial porous materials [32]. A recent review by Blunt et al. [9] describes the most common approaches to simulate flow and transport at the pore-scale that are currently in use, including, e.g., pore network models, particle based methods, and direct numerical simulations of flow. Although the

✉ Jeffrey D. Hyman
jhyman@lanl.gov

[1] Computational Earth Sciences (EES-16) Earth and Enviromental Sciences Division and The Center for Nonlinear Studies, Theoretical Division, Los Alamos National Laboratory, Los Alamos, NM 87545, USA

[2] Dipartmento di Ingegneria Civile e Ambientale, Politecnico di Milano, Piazza L. Da Vinci 32, 20133, Milano Italy

[3] Department of Hydrology and Water Resources University of Arizona Tucson, AZ 85721-0011 USA

[4] Department of Hydrology and Water Resources, Program in Applied Mathematics, University of Arizona Tucson, AZ 85721-0011, USA

differences between these approaches are considerable, they all require a representation of an explicit pore structure. In particular, when performing a direct numerical simulation of flow and transport, a detailed mesh representation of the pore space is needed to numerically integrate the governing equations [40].

Two approaches are chiefly used to obtain porous microstructures, and the choice of which is selected depends on the objectives associated with the problem of interest. The first method consists of imaging a given physical sample of a porous medium using X-ray tomography or corresponding techniques to obtain an explicit rendition of the detailed geometry of the sample pore space. Two-dimensional slices of microstructures are obtained with these techniques, reconstructed into a three-dimensional gray scale volume, and then segmented into a binary representation of the pore space that is comprised of a solid and a void phase [33, 44]. While this approach provides high-resolution images of an actual rock sample, its usefulness in characterizing effective properties driving flow and transport at a continuum scale is somewhat limited. This is primarily because the number of realizations that can be obtained and studied is constrained by the availability of rock samples, the costs of imaging, and errors that arise in image processing [18, 23]. An approach that can be employed to quantify the way the uncertainty associated with pore-scale geometry propagates to estimates of such effective continuum scale properties and their associated uncertainty relies on the generation of multiple random pore spaces that are drawn from populations with specified geometrical and topological properties. In contrast to the imaging of a real rock sample where only a single geometry is obtained, stochastic generation produces numerous pore-structures which are statistically equivalent and can be used in conjunction with efficient flow solvers to determine the effect of particular geometric observables on effective flow and transport properties.

Stochastic methods for generating porous microstructures differ according to their computational efficiency and the number of parameters that can be controlled. In general, there are three classes of stochastic pore space generation methods that are commonly used. The first prescribes particular attributes, such as porosity or grain distribution, and randomly places geometric objects, such as cubes or spheres, into a domain until target values of those attributes are obtained [5, 12, 28, 37, 43]. The second-generation method relies on statistical quantities obtained from images, e.g., two-point correlation functions or linear path functionals, obtained from images of real pore spaces to reconstruct samples with similar characteristics [4, 8, 24, 27, 29, 31, 46]. The third class of methods is based on thresholding random fields where an n-dimensional correlated topography is thresholded to produce an $(n-1)$-dimensional pore structure [22, 25, 42].

Characterization of the extent at which randomly generated pore spaces can be considered as representative of a particular rock sample depends on the metrics employed to compare the virtual sample against its physical counterpart. Typically, comparisons of patterns of geometric observables, e.g., porosity and specific surface area, macro-scale flow parameters, e.g., permeability, or autocorrelation functions are used to validate the representativeness of a virtual sample, and thereby to assess the quality of the generation method. Recently, Guadagnini et al. [13] observed scale dependence of statistics of geometric characteristics, i.e., porosity (ϕ) and specific surface area (SSA), in millimeter scale samples of natural porous media. Following typical procedures employed in statistical scaling analyses, these authors (a) consider scaling of increments, or changes, in these geometric observables across a set of length scales, ranging from the (micron) resolution scale up to the (millimeter) scale of the rock sample, and (b) ground their analysis on the computation of order q sample structure functions (statistical moments of absolute increments) of ϕ and SSA. They document the occurrence of (a) apparent power-law scaling behavior of such sample structure functions over a range of lags within the analyzed digitized porous media images, as well as (b) extended power-law scaling, assessed via extended self-similarity (ESS), the latter appearing to be an intrinsic property associated with the statistical scaling behavior of both porosity and SSA at the scale of investigation. Siena et al. [38] then show that statistical scaling of Lagrangian velocities computed numerically within the same rock samples takes place within the same range of separation scales (or lags) as for ϕ and SSA. The proper reproduction of these scaling behaviors and attributes provides another key metric that can be used to judge a generator's ability to produce realistic samples. In particular, the estimate of the Hurst coefficient, which is typically employed as an indicator of the degree of roughness (i.e., tendency for large and small values to alternate mildly or rapidly in space or time) of a target quantity and is related to its fractal dimension, serves as a quantitative measure by which to compare virtual and physical media.

In this paper, we analyze scale statistics of porosity and specific surface area of pore spaces generated according to the method of Smolarkiewicz and Winter [42] and Hyman and Winter [22]. The generation method consists of thresholding a correlated random topography, which is generated by convolving a random field with a prescribed kernel that determines the correlation structure of the topography, to produce a three-dimensional structure composed of interconnected pores embedded in an impermeable solid phase. Hyman and Winter [22] provide a rigorous theoretical investigation of the method that is complemented by an extensive

set of detailed numerical simulations on the way the generation parameters of the method control pore space geometric observables, namely: ϕ; SSA; and mean curvature. These authors also provide extensions of the method to generate pore spaces with anisotropy and multiple pore structures. Virtual pore spaces generated using this particular method were used to investigate the influence of porosity on transport properties [19], porosity, and mean hydraulic radius on permeability [20], pore wall geometry, and network topology on local mixing [21], pore size distributions on in-pore fluid velocity distributions [41]. Proper characterization of the way key statistics of geometric observables, such as ϕ and SSA, are affected by scale can be critical in applications involving the need to quantify the effect of uncertain random pore space geometry on effective properties such as medium permeabilities which can be obtained through upscaling approaches.

The extent to which existing generation methods can reproduce statistical scaling of geometric observables found in real media, and the way such scaling manifestation can be quantitatively linked to the generation parameters is still unexplored. The objective of this work is to provide such analysis upon relying on the generation method of Smolarkiewicz and Winter [42] and focusing on scale dependence of statistics of incremental values of porosity and SSA. Our analysis is grounded on the method of moments and extended self-similarity, following the works of Guadagnini et al. [13], Guadagnini et al. [14], Riva et al. [35, 36], and Siena et al. [39].

Section 2.1 describes the generation procedure for creating the virtual pore structures. The theoretical basis underpinning our analyses, the method of moments (M), and extended self similarity (ESS), are discussed in Section 2.2. An example is provided in Section 3 to illustrate the application of M and ESS in the context of a stochastically generated porous microstructure. The dependence of observed power-law scaling of q-order structure functions is then related to the generation parameters in Section 4.1, and the dependence of the estimated Hurst coefficient characterizing ϕ and SSA on the generation parameters is explored computationally in Section 4.2. We conclude with a few remarks in Section 5.

2 Experimental data and theoretical basis

A description of the adopted generation procedure to produce virtual pore spaces is first provided. A complete treatment of the method including statistics and look up tables for average (expected) values of three of the four Minkowski functionals for a porous sample [16, 17], i.e., porosity, specific surface area, and mean curvature, along with topological properties, local and global connectivity, are provided in Hyman and Winter [22]. Only a brief description of the method, and the influence of the generation parameters on porosity and specific surface area, is provided here for completeness. After describing the generation method, the theoretical underpinnings of the statistical scaling method of analysis are provided. For this purpose, we follow Guadagnini et al. [13] closely and refer the interested reader there for a complete treatment of the subject along with additional references. The section concludes with an example of application of the method of moments and extended self similarity on a porous medium sample.

2.1 Generation procedure

The generation of these microscopic pore structures is based upon level set percolation [2, 3] where locations in a random correlated topography T are mapped into the void/solid phase depending upon the height of the topography at each location. First, every node on a three-dimensional regular grid with uniform spacing δx is assigned an independent identically distributed random value sampled from a continuous uniform distribution on the closed interval $[0, 1]$, $u(\mathbf{x})$. Next, this random field is convolved with a symmetric Gaussian kernel, $k(\mathbf{x})$, to generate the isotropic correlated random topography, $T = k * u$. The Gaussian kernel has an intrinsic length scale λ which dictates the correlation length in the topography. The central limit theorem ensures that values of $T(\mathbf{x})$ are normally distributed [22]. Thresholded Gaussian fields have also been used to generate pore spaces with specific correlation structures by [1, 34, 45]. In those applications, the kernel is selected to reproduce the desired correlation structure.

After T is created, a level threshold, $\gamma \in [0, 1]$, is applied to T to determine which nodes are in the void space and which are in the solid matrix. If the value at a node is greater than γ, then the node is placed in the solid matrix; nodes with values below γ are placed in the void space. Intuitively, as γ increases so does the volume of the void space in the porous medium. The result of applying this technique is a statistically stationary pore space in the sense that the finite-dimensional probability distributions of pore space membership are invariant with respect to translation in space.

The two generation parameters, λ and γ, control the correlation structure of the topography and volume of the pore space. Larger values of λ increase the width of the Gaussian kernel, which increases the correlation length in the topography, and results in wider pores once the level threshold, γ, is applied. As γ increases, more of the topography is below the level threshold and is mapped into the void space. Thus, as γ increases so does the porosity. Porosity (ϕ), the ratio of pore volume over total volume, depends linearly on γ at intermediate values, $0.40 \leq \gamma \leq 0.60$. Hyman and Winter

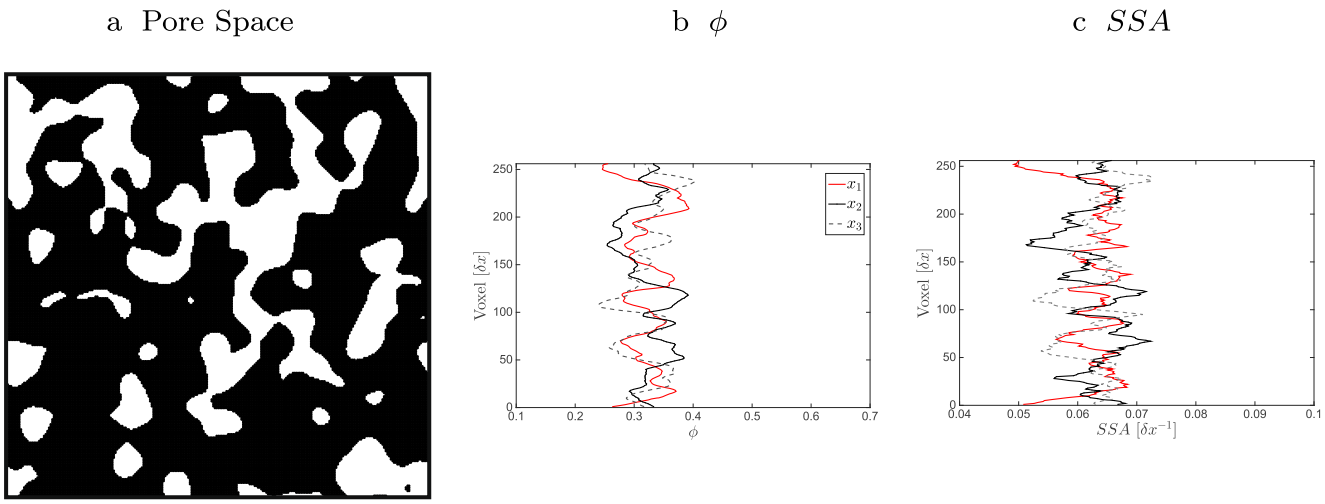

Fig. 1 **a** Horizontal cross section of pore space sample, *black* indicates solid matrix and *white* void space. Directional profiles of porosity (ϕ) (**b**) and specific surface area (SSA) (**c**). *Colors* indicate different coordinate axes

[22] show that over the entire range of threshold values, the porosity is determined via a complementary error function which depends upon both γ and λ. The specific surface area (SSA), the total interstitial area (per unit volume) between the pore space and the solid matrix, depends nonlinearly on both γ and λ. Small values of λ create a more rugged topography, which results in numerous narrow pores with higher surface area than topographies generated with larger correlation lengths, which produce realizations with wider pores. At a fixed value of λ, the values of SSA are nearly symmetric about $\gamma = 0.50$, rising with γ increasing from 0.40 to 0.50, and decreasing when γ increases from 0.50 to 0.60.

The grid resolution, δx, determines the spatial resolution of the pore structure. Most of the samples used in this study are unit volumes of L^3 and $\delta x = L/N$, where N is the number of voxels in one spatial dimension. This generality allows for the method to be used at a wide range of spatial scales, and the presented results hold for arbitrary spatial resolutions. When a sample is not a unit volume, it is clearly noted.

2.2 Method of moments and extended self similarity

We investigate power-law scaling of order q sample structure functions, defined as

$$S_N^q(s_i) = \frac{1}{N(s_i)} \sum_{n=1}^{N(S)} |\Delta y_n(s_i)]^q \ , \tag{1}$$

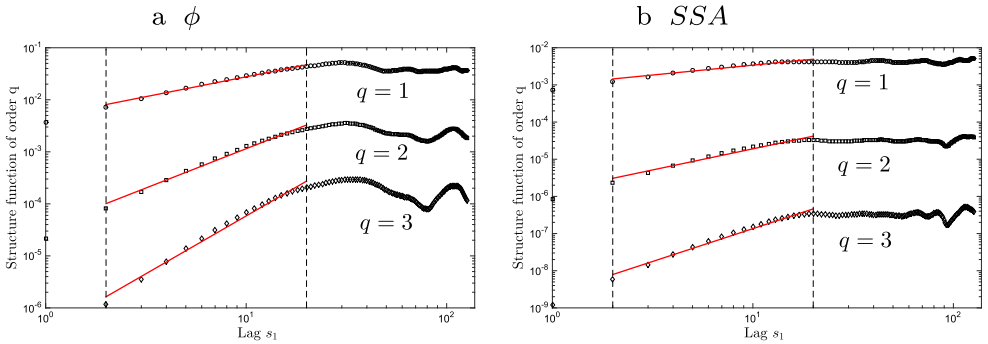

Fig. 2 Structure functions of order $q = 1, 2, 3$ for porosity (ϕ) (**a**) and specific surface area (SSA) (**b**) parallel to x_1. Power-law fits are determined by maximizing the coefficient of determination R^2. *Dashed lines* indicate the range of lags where power-law scaling is observed. In a low to mid-range of lags, which extends for about a decade within the observation window of the investigated domain, each structure function scales as a power of lag, a feature which has also been observed in imaged real rock samples at the millimeter scale by Guadagnini et al. [13]

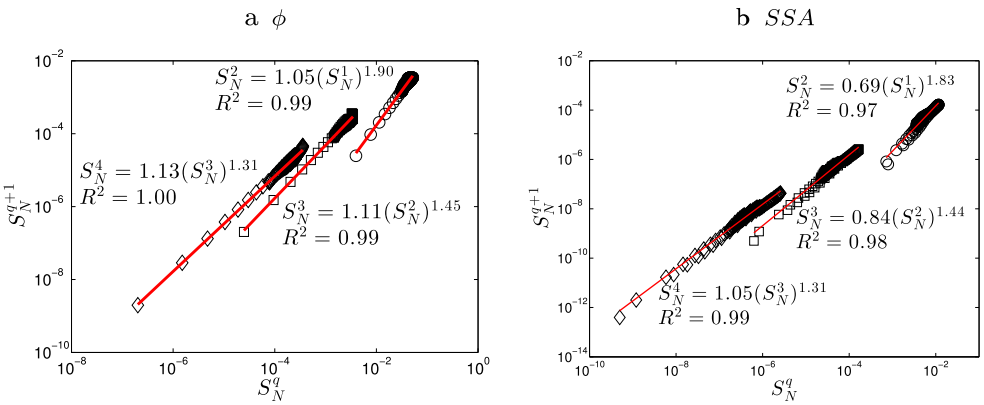

Fig. 3 Dependence of S_N^{q+1} on S_N^q for q = 1, 2, 3 for porosity (ϕ) (**a**) and specific surface area (SSA) (**b**) parallel to x_1. Regression lines are fitted to the curves are shown in *red*. The linear relationship between the sequential structure functions reveals that S_N^q exhibits extended power-law scaling at all lags

where $y(x)$ is a realization of a random field $Y(x)$ defined on a continuum of points x in a one-dimensional setting. Here, $Y(x)$ is either ϕ or SSA calculated for volumes of planar extent $L \times L$ and unit voxel thickness, parallel to the three Cartesian axis, x_i for $i = 1, 2$, and 3, and $\Delta y_n(s_i) = y(x_{i,n}+s_i) - y(x_{i,n})$ is an increment of $y(x_i)$ calculated over a lag (s_i) between two points along the direction x_i, $N(s_i)$ being the number of such increments. Power-law scaling as a function of lag is defined as

$$S_N^q(s_i) \propto s_i^{\xi_i(q)} \tag{2}$$

where the power or scaling exponent, $\xi_i(q)$, can vary with direction x_i, and is independent of s_i.

Using these structure functions, we identify and analyze power-law scaling of ϕ and SSA through the method of moments (M) and extended self-similarity (ESS) for virtual samples generated using the method mentioned above, cf. Siena et al. [39] for details and references about M and ESS.

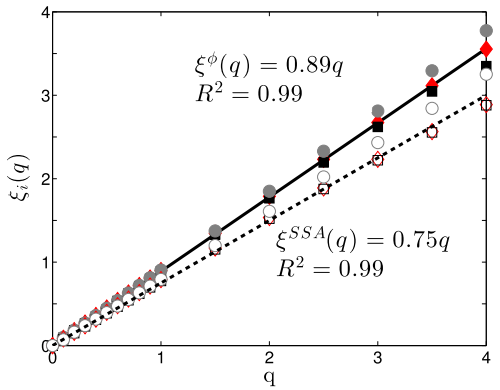

Fig. 4 Directional dependence of $\xi_i(q)$, x_1 (*red diamonds*), x_2 (*black squares*) , x_3 (*grey circle*) on q obtained through ESS for porosity (ϕ) (*filled markers*) and specific surface area (SSA) (*empty markers*). Linear fits and R^2 values are also provided for ϕ (*solid line*) and SSA (*dashed line*). No significant directional dependence is observed because the underlaying topography is isotropic. The slope of the linear regression lines provides an estimate for the Hurst coefficient. The estimated Hurst scaling exponents for this sample, $\widehat{H}_{\phi} = 0.89$ for ϕ and $\widehat{H}_{SSA} = 0.75$ for SSA, are close to those reported by [13] for natural samples of sandstone

In the method of moments, the sample structure functions (1) are inferred for a set of lags and a series of q_i values $i = 1, 2, \ldots, n$. The structure function $S_N^{q_j}$ is plotted against s_i on a log-log scale. A linear, or near-linear dependence of $\log S_N^{q_j}$ on $\log s_i$ is usually obtained within an intermediate range of lags, $s_I < s_i < s_{II}$, where the upper and lower limits s_I and s_{II} are defined theoretically or, more commonly, empirically. The power $\xi_i(q_j)$ ($j = 1, 2, \ldots, n$) is the slope of this linear regression. Benzi et al. [7] and Benzi et al. [6] introduced ESS as an empirical procedure to extend power-law scaling at all separation scales by observing that

$$S_N^n(s_i) \propto S_N^m(s_i)^{\beta_i(n,m)}, \tag{3}$$

where $\beta_i(n, m) = \xi(n)/\xi(m)$ is the ratio between the scaling exponents of $S_N^n(s_i)$ and $S_N^m(s_i)$.

A theoretical basis for Eq. 3 has been given in the context of (a) the one-dimensional Burger equation [10], (b) Gaussian random fields constituting a sample from a truncated fractional Brownian motion (tfBm), or truncated fractional Gaussian noise (tfGn) [39], and (c) sub-Gaussian random processes subordinated to tfBm or tfGn [15, 30]. The latter fields constitute mixtures of Gaussian fields with random variance and are consistent with typical power-law scaling at intermediate lags and with ESS at all lags.

3 Example of scaling of porosity and specific surface increments

A sample realization of a pore space is generated using an intrinsic length scale $\sqrt{\lambda} = 0.025$ and level threshold of $\gamma = 0.45$. The unit cube is discretized using 256^3 voxels. Figure 1a shows a horizontal cross section of the pore space sample; Fig. 1b, c depict the profiles of porosity ϕ and specific surface area SSA for the sample realization in all three primary directions, x_1, x_2, and x_3. These directional profiles are calculated following [13] and relying on the algorithms of [11]. As a reference, the bulk porosity of the sample is ≈ 0.32 and the specific surface area is $0.0953\ \delta x^{-1}$.

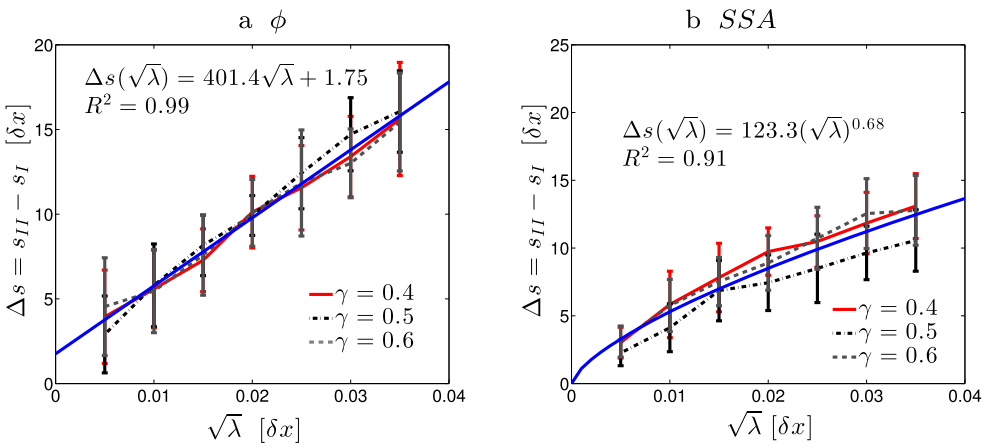

Fig. 5 Length of lags where power-law scaling of structure functions (1) for porosity (ϕ) (**a**) and specific surface area (SSA) (**b**) plotted as functions of $\sqrt{\lambda}$, the intrinsic length scale of the Gaussian kernel. Different level thresholds, γ, are denoted by γ = 0.4 (*red solid*), γ = 0.5 (*black dots*) , γ = 0.6 (*gray, dot-dashed*). A linear model for porosity and a power-law model for SSA are shown in *blue*

The Lillie test indicates that the empirical probability distributions of porosity and SSA are most likely Gaussian, this hypothesis is not rejected at the 5 % significance level. The same holds for the distributions of their incremental values at diverse lags. These results are also confirmed for a wide range of generation pairs, $0.005 \leq \sqrt{\lambda} \leq 0.035$ and $0.40 \leq \gamma \leq 0.60$ (details not provided).

Absolute increments of ϕ and SSA are computed for lags $s_i \leq 128$. Thus, the number of samples employed for the evaluation of each structure function (1) ranges from 255 to 128, ensuring that a sufficient number of samples is obtained for an estimation of the structure functions. Figure 2a shows the logarithm of the structure functions of order $q = 1$, 2, and 3 for porosity and Fig. 2b shows the same quantities for SSA, both computed parallel to the x_1 plane, plotted against the logarithm of lag s_1. Dashed lines in the figures indicate the approximate maximum range of lags s_1 where power-law scaling behavior can be observed, $s_I < s_1 < s_{II}$. The lower and upper scaling bounds, respectively indicated as s_I and s_{II}, are computed in two steps. First, a possible value for s_{II} is determined by finding the smallest (directional) lag value such that the second derivative of the spline interpolant of the structure function is below a user-prescribed tolerance. Using this value as an initial guess, a search is performed to determine the values of s_I and s_{II} which maximizes the coefficient of determination (R^2) of the linear regression. In all of the cases shown, R^2 is greater than 0.98.

As described in Section 2.2, the method of moments (M) uses the plots of $\log S_N^{q_j}$ for $j = 1, 2, \ldots, n$ against $\log s_i$ to determine a linear relationship between the two (Fig. 2) over the range $s_I < s_1 < s_{II}$. The scaling exponent, $\xi(q)$, is estimated as the slope of the regression line over this region. We found $s_I = 2$ and $s_{II} = 17$ for ϕ and $s_I = 2$ and $s_{II} = 15$ for SSA in this example. The results suggest that in a low to mid-range of lags, which extends for about a decade within the observation window of the investigated domain, each structure function scales as a power of lag, a feature which has also been observed in imaged real rock samples at the millimeter scale by Guadagnini et al. [13]. The width of these scaling regions depends upon the intrinsic length scale of the Gaussian kernel, λ; this dependence is systematically explored in Section 4.1.

Figure 3 depicts the dependence of $\log(S_N^{q+1})$ on $\log(S_N^q)$ which is obtained through application of ESS to the quantities displayed in Fig. 2 for ϕ (a) and SSA (b) computed along the x_1 direction. The linear relationship between sequential structure functions reveals that S_N^q exhibits extended power-law scaling at all lags.

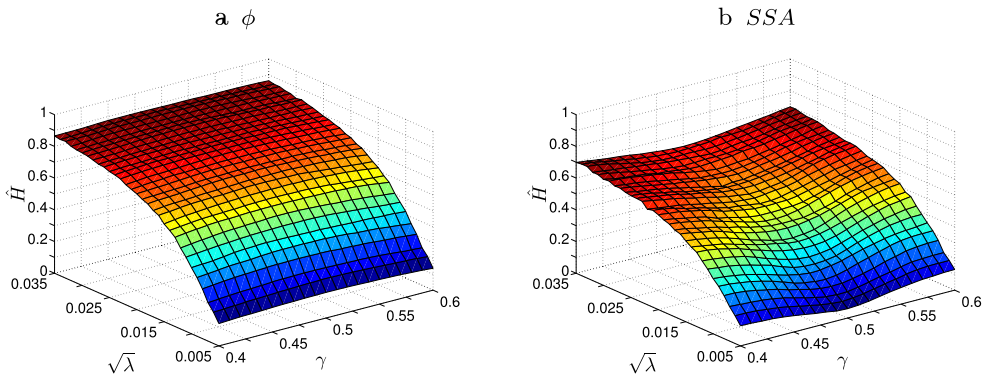

Fig. 6 Average estimated Hurst coefficient for incremental values of porosity (ϕ) (**a**) and specific surface area (SSA) (**b**). A nonlinear model of the form $\widehat{H}(\gamma, \lambda) = a(\gamma - 0.5)^2 + b\log(\sqrt{\lambda}) + c$ fits the surfaces well. Parameters for the model are provided in Table 1

Regression lines which are fitted to the curves are also depicted in Fig. 3, together with the associated expressions and coefficient of determination, (R^2). The latter is always at least 0.97.

A symmetric Gaussian kernel is used in the construction of the example topography and therefore the topography, and the induced pore space, is isotropic and stationary. Hence, there should not be directional dependence of $\xi_i(q)$ on x_i. Indeed, this is observed by plotting $\xi_i(q)$ $(i = 1, 2, 3)$ against q for the sample realization. Values of $\xi_i(q)$ are computed using values of q ranging from $0.1 \leq q \leq 1$ in increments of $\Delta q = 0.1$ and then from $1 \leq q \leq 4$ in increments of $\Delta q = 0.5$ for all three directions. All of the values are plotted against q and for $\xi_i(q)$ $(i = 1, 2, 3)$ in Fig. 4 for both ϕ (filled markers) and SSA (empty markers). The pore topography can be rendered anisotropic by using an asymmetric kernel in the convolution. This anisotropy will then be observed in the range of lags associated with power-law scaling and in the slope of the regression line (not shown). By varying the kernel in this manner, the anisotropy that has been observed in natural samples [13] can be created.

A linear relationship between the scaling exponent ξ and q is observed for both ϕ and SSA that persists over the entire sampled space of q values. When the scaling exponent $\xi(q)$ is linearly proportional to q, $Y(x)$ is typically interpreted as a (mono-fractal) self-similar random process with Hurst exponent H [13] (and references therein). The slope of the linear regression lines provides an estimate for the Hurst coefficient. The estimated Hurst scaling exponents for this sample, $\widehat{H}_\phi = 0.89$ for ϕ and $\widehat{H}_{SSA} = 0.75$ for SSA, are close to those reported by [13] for natural samples of sandstone.

4 Dependence of statistical scaling on generation parameters

The generation parameters, the intrinsic length scale of the kernel λ and the level threshold γ, determine the volume and structure of the pore space. Therefore, they also determine the statistical scaling of ϕ and SSA. In this section, we determine empirical relationships between the generation parameters and (a) the length of the range of lags where power-law scaling of the sample structure functions is observed and (b) the estimated Hurst coefficient.

4.1 Power-law scaling length

The range of lags where power-law behavior of the sample structure functions is observed (delimited by the dashed vertical lines in Fig. 2) depends upon the intrinsic length scale of the kernel λ and the level threshold γ. To quantify this dependence, 1350 samples with dimensions $256 \times 256 \times 2048$ are generated using $0.005 \leq \sqrt{\lambda} \leq 0.035$ with $\Delta\sqrt{\lambda} = 0.005$ and $0.40 \leq \gamma \leq 0.60$ with $\Delta\gamma = 0.10$. The structure functions are computed in the x_3 direction, with $s_3 \leq 1024$. This results in large sample sizes, ranging from 2047 to 1023 elements for the set of lags considered, and leads to accurate estimates of the structure functions. The average values of the length of the interval of lags, $\Delta s = s_{II} - s_I$, where power-law behavior is observed along with error bars are plotted against $\sqrt{\lambda}$ for three selected values of γ in Fig. 5a for ϕ and Fig. 5b for SSA.

With regard to porosity, a linear relationship between $\sqrt{\lambda}$ and Δs is observed, the results appearing to be insensitive to the level threshold γ. A linear model $\Delta s(\sqrt{\lambda}) = m\sqrt{\lambda} + b$ where $m = 401.4$ $(379.2, 423.6)$ and $b = 1.754$ $(1.26, 2.25)$ fits the data well (here and in the following, values in parenthesis indicate bounds of nominal 95 % confidence intervals). The linear model depicted in the figure is associated with values of $R^2 = 0.99$. In contrast, the length of the interval of lags where structure functions of SSA exhibit power-law scaling depends nonlinearly on both $\sqrt{\lambda}$ and γ (Fig. 5b). A power-law model captures the nonlinear dependence of Δs on $\sqrt{\lambda}$, and is plotted along with the data as a solid blue line. The model $\Delta s(\sqrt{\lambda}) = a(\sqrt{\lambda})^b$ where $m = 123.3$ $(65.19, 181.3)$ and $b = 0.68$ $(0.56, 0.81)$ fits the data well, being associated with $R^2 = 0.91$. As noted in Section 2.1, the expected value of SSA is a nonlinear function of γ and is symmetric about $\gamma = 0.50$. Consistent with this, it can be seen that the average values of Δs obtained for $\gamma = 0.4$ and $\gamma = 0.6$ and depicted in (Fig. 5b) are virtually indistinguishable. On the other hand, our results show that values obtained for $\gamma = 0.5$ are visibly lower.

4.2 Estimated Hurst coefficient

Here, we analyze the way the estimated values of the Hurst scaling exponent [26] observed for ϕ and SSA are related to the model generation parameters. We do so by quantifying the dependence on the model generation parameters of average values of estimations for the Hurst coefficients for porosity ($\widehat{H}_\phi$) and specific surface area ($\widehat{H}_{SSA}$) over a large set of virtual samples. As noted in Section 1, the Hurst exponent provides an indication of the type of spatial dependence of the increments of given quantities, and is therefore of particular interest in stochastic analyses of flow and transport in porous media.

The mean and variance of $\widehat{H}$ estimates are computationally determined by generating a total of 166,656 independent realizations of virtual media and computing the associated Hurst scaling coefficients; the slope of the linear

Table 1 Computationally determined average values (subscript μ) of the Hurst coefficient for porosity (ϕ) and specific surface area (SSA) along with variance of sample sets (subscript σ^2; values are $\cdot 10^{-3}$)

	γ : 0.40		γ : 0.50		γ : 0.60	
$\sqrt{\lambda}$	ϕ_μ	SSA_μ	ϕ_μ	SSA_μ	ϕ_μ	SSA_μ
0.0050	0.13	0.13	0.16	0.06	0.14	0.13
0.0150	0.62	0.51	0.66	0.35	0.62	0.52
0.0250	0.79	0.64	0.81	0.54	0.79	0.64
0.0350	0.87	0.70	0.87	0.62	0.86	0.70
$\sqrt{\lambda}$	ϕ_{σ^2}	SSA_{σ^2}	ϕ_{σ^2}	SSA_{σ^2}	ϕ_{σ^2}	SSA_{σ^2}
0.0050	4.72	4.18	5.83	1.56	4.99	4.57
0.0150	8.41	9.81	5.33	1.06	9.81	8.01
0.0250	3.95	9.89	4.09	9.48	4.51	7.92
0.0350	3.37	7.12	3.48	8.52	3.05	8.43

regression line for the scaling exponent ξ as a function of q is used as an estimate for the Hurst coefficient. Generation pairs comprised of 31 values of $0.005 \leq \sqrt{\lambda} \leq 0.035$ and 21 values of $0.40 \leq \gamma \leq 0.60$ are used. For each generation pair, 256 independent realizations are generated. Here, only values calculated for the direction x_1 are reported because the other two directions provide statistically identical values, cf. Section 3. $\widehat{H}$ are provided in Fig. 6a for porosity and Fig. 6b for SSA. Average values and variances of the sample set at selected generation pairs are listed in Table 1. Estimates $\widehat{H}$ depend nonlinearly on both the intrinsic length scale of the kernel λ and the level threshold γ. For both ϕ and SSA, at a fixed γ, the $\widehat{H}$ coefficient increases logarithmically with rising values of $\sqrt{\lambda}$. At a fixed level of λ, the Hurst coefficient exhibits a quadratic trend with a vertex at $\gamma = 0.50$. The surface of $\widehat{H}_\phi$, is a convex function of γ, while the surface $\widehat{H}_{SSA}$, is a concave function of γ.

The three parameter model,

$$\widehat{H}(\gamma, \lambda) = a(\gamma - 0.5)^2 + b \log(\sqrt{\lambda}) + c \,, \tag{4}$$

provides high fidelity estimates of the average estimated Hurst scaling coefficient for both ϕ and SSA. Model parameter values are estimated using maximum likelihood estimations and are listed in Table 2, along with the corresponding nominal 95 % confidence bounds, and standard goodness of fit criteria (SSE: sum of squared errors, RMSE: root mean squared error). An alternative model formulation that included an interaction term of the kind $(\gamma\sqrt{\lambda})^d$ did not increase the accuracy of the corresponding estimates, the estimated value of the additional parameter d being essentially zero. Two of the parameter values in our proposed empirical model, namely the coefficient of the logarithm of $\sqrt{\lambda}$ (b) and the constant term (c), are quite similar for $\widehat{H}_\phi$ and $\widehat{H}_{SSA}$. However, one can note that the leading coefficients of the quadratic terms are notably different in both magnitude and sign to capture the concavity of the surface describing the Hurst coefficient in the generation parameter space.

5 Conclusions

Our works leads to the following major conclusions.

1 By computing order q structure functions (statistical moments of absolute increment) of porosity and specific surface area of three-dimensional stochastically generated porous microstructures, we demonstrate that the generation method of Smolarkiewicz and Winter [42] and Hyman and Winter [22] qualitatively and quantitatively reproduces salient features of statistical scaling behavior observed in real rock samples.

Table 2 Empirical model for the maximum likelihood estimates of the Hurst coefficient $\widehat{H}$: $\widehat{H}(\gamma, \lambda) = a(\gamma - 0.5)^2 + b \log(\sqrt{\lambda}) + c$ along with nominal confidence intervals and goodness of fit metrics (SSE sum of squared errors, R^2 coefficient of determination RMSE root mean squared error)

	Coefficients	95 % confidence bounds:	Goodness of fit:
Porosity ($\widehat{H}_\phi$)	a = −2.75	(−3.52, −1.99)	SSE: 0.69
	b = 0.39	(0.38, 0.39)	R^2: 0.98
	c = 2.22	(2.20, 2.24)	RMSE: 0.03
SSA ($\widehat{H}_{SSA}$)	a = 11.37	(10.89, 11.85)	SSE: 0.27
	b = 0.30	(0.29, 0.31)	R^2: 0.99
	c = 1.66	(1.64, 1.67)	RMSE: 0.020

2 The observed linear variation of the scaling exponent $\xi(q)$ for the range of q values analyzed is consistent with the nature of the generation method, which creates Gaussian random fields that are thresholded to produce the pore spaces. This observation is also consistent with numerical results of Guadagnini et al. [14].

3 The order q sample structure functions are computed across a variety of generated pore spaces and for a wide range of combinations of the generation parameters scale as a power of the separation distance or lag over an intermediate range of lags. Extended power-law scaling, also termed extended self-similarity (ESS), appears to be an intrinsic property of the virtual media we generate and analyze. These results are consistent with observations based on the analysis of millimeter scale natural rock samples imaged at the micron-scale resolution.

4 The length of the range of lags where power-law scaling is observed and the Hurst coefficient can be controlled by the generation parameters of the method. We provide empirical relationships to guide the generation of random pore spaces associated with given values of these two quantities.

5 Our results show that the generation method is capable of rendering pore space geometries characterized by distributions of porosities and SSA which can be anti-persistent (with a tendency of large and low values to alternate rapidly in space, in a rough rather than smooth manner) or persistent in space, respectively associated with values of the Hurst coefficient that are lower or larger than 0.5 for the Gaussian systems analyzed. While in their analysis of real rock samples, Guadagnini et al. [13] show that that ϕ and SSA are generally associated with a mild to strong persistent behavior, varying in a smooth fashion, i.e., with a tendency for large and small values to alternate mildly over space, it has to be noted that the analysis of statistical scaling of geometric observables at such small scales $\mathcal{O}(\mu m)$ are still in their infancy. As such, the ability of having a virtual pore space generation procedure with such a broad range of generation capabilities can be critical for applications involving the analysis of fluid flow and solute transport in complex natural pore spaces.

Remark Our ability of rendering virtual pore samples displaying scale-dependence of statistics of geometric characteristics of the kind which has been documented for imaged pore spaces of real rocks [13] depends on the particular generation methodology employed. Here, we have demonstrated that (a) the approach we adopt can lead to the generation of a population of samples displaying such scaling patterns, and (b) the generation parameters contain information about the way one can reproduce in the population of the generated samples the width of the range of lags where such scaling is manifested in the real medium. Samples generated using other approaches, or even other kernels in the convolution to create the correlated random topography, may or may not exhibit such scaling. A comparison of the type of scale dependence of statistics of geometric characteristics is another measurement by which one can judge the representativeness of a synthetic sample.

All of the virtual samples analyzed in this work are produced using a symmetric Gaussian kernel to construct the random topography. The resulting pore spaces are isotropic, and thus there is no directional dependence observed for the scaling exponent $\xi(q)$ or the Hurst coefficient. To capture the anisotropy which might be seen in some natural samples, an anisotropic kernel can be used in the generation procedure, as described in [22]. We further note that real pore spaces might exhibit multiple pore structures with pores of various sizes and orientations, a feature which can be included in the generation, as discussed in Hyman and Winter [22], but was not done here for simplicity and clarity. However, in doing so, two pore spaces with different Hurst coefficients are merged. Thus, it might be possible to create pore spaces whose Hurst coefficient does not scale linearly over the range of q values considered using these pore spaces. Exploring and determining how the generation procedure can control this non-linearity is the subject of ongoing research. Finally, it should be possible to use colored noise for the generation of the underlying random field and create topographies that are non-Gaussian. This extension of the method is also the subject of ongoing research.

Acknowledgments JDH gratefully acknowledges the support of the U.S. Department of Energy through the LANL/LDRD projects 20140002DR and grant no. DE-AC52-06NA25396 for this work. AG gratefully acknowledges funding from MIUR (Italian ministry of Education, Universities and Research- PRIN2010-11; project: "Innovative methods for water resources under hydro-climatic uncertainty scenarios").

References

1. Adler, P.M., Jacquin, C.G., Quiblier, J.A.: Flow in simulated porous media. Int J. Multiphas Flow **16**(4), 691–712 (1990)
2. Alexander, K.S.: Percolation and minimal spanning forests in infinite graphs. Ann. Probab, 87–104 (1995)
3. Alexander, K.S., Molchanov, S.A.: Percolation of level sets for two-dimensional random fields with lattice symmetry. J. Stat. Phys. **77**(3), 627–643 (1994)
4. Arns, C.H., Knackstedt, M.A., Mecke, K.R.: Reconstructing complex materials via effective grain shapes. Phys. Rev. Lett. **91**(21), 215–506 (2003)
5. Balhoff, M.T., Thomas, S.G., Wheeler, M.F.: Mortar coupling and upscaling of pore-scale models. Computat. Geosci **12**(1), 15–27 (2008)

6. Benzi, R., Ciliberto, S., Baudet, C., Chavarria, G.R., Tripiccione, R.: Extended self-similarity in the dissipation range of fully developed turbulence. EPL Europhys. Lett. **24**(4), 275 (1993)
7. Benzi, R., Ciliberto, S., Tripiccione, R., Baudet, C., Massaioli, F., Succi, S.: Extended self-similarity in turbulent flows. Phys. Rev. E **48**(1), R29 (1993)
8. Biswal, B., Held, R.J., Bakke, S., Hilfer, R.: Modeling of multiscale porous media. Image Anal Stereol **28**, 23–34 (2009)
9. Blunt, M.J., Bijeljic, B., Dong, H., Gharbi, O., Iglauer, S., Mostaghimi, P., Paluszny, A., Pentland, C.: Pore-scale imaging and modelling. Adv. Water Resour. **51**, 197–216 (2013)
10. Chakraborty, S., Frisch, U., Ray, S.S.: Extended self-similarity works for the Burgers equation and why. J. Fluid Mech. **649**, 275–285 (2010)
11. Coker, D.A., Torquato, S.: Extraction of morphological quantities from a digitized medium. J. Appl. Phys. **77**(12), 6087–6099 (1995)
12. Duda, A., Koza, Z., Matyka, M.: Hydraulic tortuosity in arbitrary porous media flow. Phys. Rev. E **84**(3), 036–319 (2011)
13. Guadagnini, A., Blunt, M., Riva, M., Bijeljic, B.: Statistical scaling of geometric characteristics in millimeter scale natural porous media. Trans. Porous Med. **101**(3), 465–475 (2014)
14. Guadagnini, A., Neuman, S.P., Riva, M.: Numerical investigation of apparent multifractality of samples from processes subordinated to truncated fBm. Hydrol. Processes **26**(19), 2894–2908 (2012)
15. Guadagnini, A., Riva, M., Neuman, S.P.: Extended power-law scaling of heavy-tailed random air-permeability fields in fractured and sedimentary rocks. Hydrol. Earth Syst Sci **16**(9), 3249–3260 (2012)
16. Hilfer, R.: Local porosity theory and stochastic reconstruction for porous media. In: Statistical Physics and Spatial Statistics, pp. 203–241. Springer (2000)
17. Hilfer, R.: Review on scale dependent characterization of the microstructure of porous media. Trans. Porous Media **46**(2–3), 373–390 (2002)
18. Hilfer, R., Zauner, T.: High-precision synthetic computed tomography of reconstructed porous media. Phys. Rev. E **84**(6), 062–301 (2011)
19. Hyman, J.D., Smolarkiewicz, P.K., Winter, C.: Heterogeneities of flow in stochastically generated porous media. Phys.Rev. E **86**, 056–701 (2012). doi:10.1103/PhysRevE.86.056701
20. Hyman, J.D., Smolarkiewicz, P.K., Winter, C.L.: Pedotransfer functions for permeability: a computational study at pore scales. Water Resour. Res. **49** (2013). doi:10.1002/wrcr.20170
21. Hyman, J.D., Winter, C.L.: Hyperbolic regions in flows through three-dimensional pore structures. Phys. Rev. E **88**, 063–014 (2013)
22. Hyman, J.D., Winter, C.L.: Stochastic generation of explicit pore structures by thresholding Gaussian random fields. J Comput. Phys. **277** (0), 16–31 (2014)
23. Iassonov, P., Gebrenegus, T., Tuller, M.: Segmentation of X-ray computed tomography images of porous materials: a crucial step for characterization and quantitative analysis of pore structures. Water Resour. Res **45**, 9 (2009)
24. Latief, F.E., Biswal, B., Fauzi, U., Hilfer, R.: Continuum reconstruction of the pore scale microstructure for fontainebleau sandstone. Physica A **389**(8), 1607–1618 (2010)
25. Lemaitre, R., Adler, P.M.: Fractal porous media iv: three-dimensional Stokes flow through random media and regular fractals. Transport in Porous Med. **5**(4), 325–340 (1990)
26. Mandelbrot, B.B., Van Ness, J.W.: Fractional Brownian motions, fractional noises and applications. SIAM Rev **10**(4), 422–437 (1968)
27. Manwart, C., Torquato, S., Hilfer, R.: Stochastic reconstruction of sandstones. Phys. Rev. E **62**, 893–899 (2000). doi:10.1103/PhysRevE.62.893
28. Matyka, M., Khalili, A., Koza, Z.: Tortuosity-porosity relation in porous media flow. Phys. Rev. E 78 **2**(026), 306 (2008)
29. Mecke, K.R.: Integral geometry in statistical physics. Int. J. Mod. Phys. B **12**(09), 861–899 (1998)
30. Neuman, S.P., Guadagnini, A., Riva, M., Siena, M.: Recent advances in statistical and scaling analysis of earth and environmental variables. In: Advances in Hydrogeology, pp. 1–25 Springer (2013)
31. Okabe, H., Blunt, M.: Prediction of permeability for porous media reconstructed using multiple-point statistics. Phys. Rev E **70**(6), 066–135 (2004)
32. Oostrom, M., Mehmani, Y., Romero-Gomez, P., Tang, Y., Liu, H., Yoon, H., Kang, Q., Joekar-Niasar, V., Balhoff, M., Dewers, T., Tartakovsky, G., Leist, E., Hess, N., Perkins, W., Rakowski, C., Richmond, M., Serkowski, J., Werth, C., Valocchi, A., Wietsma, T., Zhang, C.: Pore-scale and continuum simulations of solute transport micromodel benchmark experiments. Computat. Geosci, 1–23 (2014)
33. Porter, M.L., Wildenschild, D., Computat. Geosci.: Image analysis algorithms for estimating porous media multiphase flow variables from computed microtomography data: a validation study **1**, 15–30 (2010)
34. Quiblier, J.A.: A new three-dimensional modeling technique for studying porous media. J.Colloid Interf. Sci **981**, 84–102 (1984)
35. Riva, M., Neuman, S., Guadagnini, A.: Sub-Gaussian model of processes with heavy-tailed distributions applied to air permeabilities of fractured tuff. Stochastic Environmental Research and Risk Assessment **27**(1), 195–207 (2013)
36. Riva, M., Neuman, S.P., Guadagnini, A., Siena, M.: Anisotropic scaling of berea sandstone log air permeability statistics. Vadose Zone Journal **12**, 3 (2013)
37. Romero, P., Gladkikh, M., Azpiroz, G. Computat. Geosci **13**(2), 171–180 (2009). doi:10.1007/s10596-008-9098-6
38. Siena, M., Guadagnini, A., Riva, M., Bijeljic, B., Nunes, J.P.P., Blunt, M.J.: Statistical scaling of pore-scale Lagrangian velocities in natural porous media. Phys. Rev. E 90 **2**(023), 013 (2014)
39. Siena, M., Guadagnini, A., Riva, M., Neuman, S.P.: Extended power-law scaling of air permeabilities measured on a block of tuff. Hydrol. Earth Syst Sci **16**(1), 29–42 (2012)
40. Siena, M., Hyman, J.D., Riva, M., Guadagnini, A., Winter, C.L., Smolarkiewicz, P.K., Gouze, P., Sadhukhan, S., Inzoli, F., Guédon, G., Colombo, E.: Direct numerical simulation of fully-saturated flow in natural porous media at the pore scale: a comparison of three computational systems. Comput. Geosci., 1–15 (2015). doi:10.1007/s10596-015-9486-7
41. Siena, M., Riva, M., Hyman, J.D., Winter, C.L., Guadagnini, A.: Relationship between pore size and velocity probability distributions in stochastically generated porous media. Phys. Rev. E **89**(003), 000 (2014)
42. Smolarkiewicz, P.K., Winter, C.L.: Pores resolving simulation of Darcy flows. J. Comput. Phys **229**(9), 3121–3133 (2010)
43. Tartakovsky, A.M., Meakin, P., Scheibe, T.D., Eichler West, R.M.: Simulations of reactive transport and precipitation with smoothed particle hydrodynamics. J. Comput. Phys. **222**(2), 654–672 (2007)
44. Wildenschild, D., Sheppard, A.P.: X-ray imaging and analysis techniques for quantifying pore-scale structure and processes in subsurface porous medium systems. Adv. Water Resour. **51**, 217–246 (2013)
45. Yao, J., Frykman, P., Kalaydjian, F., Thovert, J.F., Adler, P.M.: High-order moments of the phase function for real and reconstructed model porous media A comparison. J. Colloid Interf. Sci **156**(2), 478–490 (1993)
46. Yeong, C., Torquato, S.: Reconstructing random media. Phys. Rev. E **57**(1), 495 (1998)